

1 **Title: Metabolic turnover and dynamics of modified ribonucleosides by ^{13}C labeling**

2 **Authors:** Paulo A. Gameiro^{1,2*}, Vesela Encheva³, Mariana Silva Dos Santos³, James I MacRae³ and
3 Jernej Ule^{1,2}

4 **Corresponding author information:** paulo.gameiro@crick.ac.uk

5 **Affiliations:** ¹RNA Networks Laboratory, Francis Crick Institute, London, UK. ²Department of
6 Neuromuscular Diseases, UCL Queen Square Institute of Neurology, London, UK. ³Mass Spectrometry
7 Science Technology Platform, Francis Crick Institute, London, UK

8 **Abstract**

9 Tandem mass spectrometry (MS/MS) is an accurate tool to assess modified ribonucleosides
10 and their dynamics in mammalian cells. Yet, MS/MS quantification of lowly abundant modifications
11 in non-ribosomal RNAs is unreliable, and the dynamic features of various modifications poorly
12 understood. We developed a ^{13}C labeling approach, ^{13}C -dynamods, to quantify the turnover of base
13 modifications in newly transcribed RNA. This turnover-based approach helped to resolve mRNA from
14 ncRNA modifications in purified RNA or free ribonucleosides, and showed the distinct kinetics of *N*6-
15 methyladenosine (m^6A) versus 7-methylguanosine (m^7G) in polyA+-purified RNA. We uncovered that
16 *N*6,*N*6-dimethyladenosine (m^6_2A) exhibits a distinct turnover in small RNAs and free ribonucleosides
17 when compared to the known m^6_2A -modified large rRNAs. Finally, combined measurements of
18 turnover and abundance informed on the transcriptional versus posttranscriptional sensitivity of
19 modified ncRNAs and mRNAs, respectively, to stress conditions. Thus, ^{13}C -dynamods enables studies
20 of origin of modified RNAs at steady-state and their dynamics under non-stationary conditions.

21 **Keywords:** Isotopic labeling; RNA modifications; RNA turnover; *N*6-methyladenosine; 7-
22 methylguanosine; *N*6,*N*6-dimethyladenosine; mass spectrometry; metabolism; methylation dynamics;
23 metabolic stress

24

25

INTRODUCTION

26 RNA methylation modulates crucial RNA-protein interactions at various stages of RNA
27 metabolism. Comprehensive studies of individual RNA modifications have been mostly advanced by
28 applications of next-generation sequencing (NGS), which rely on chemical, enzymatic and/or antibody-
29 based detection of modified ribonucleosides (1–3). These methods have provided a wealth of
30 information on the sites of modification across the transcriptome (1–3), which have uncovered the
31 dynamic behavior of *N*6-methyladenosine (m⁶A) mRNA methylation in development (4–8). Notably,
32 dysregulation of m⁶A levels has been recently linked to cancer, ageing and neurodegeneration (9–15),
33 which can occur via metabolic inhibition of m⁶A demethylation (9, 10). Furthermore, various tRNA
34 modifications have been reported to be post-transcriptional sensitive to cellular stress (16–19). A current
35 caveat of NGS-based profiling is the lack of high specificity reagents for every modification (1–3).
36 Also, the effects of transcription, which often predominate in differential expression analyses (20),
37 make it challenging to quantify general changes in methylation levels, with limited insight being
38 obtained into biological associations between various modifications. As a consequence, the dynamic
39 behavior of RNA methylation often remains poorly understood, and complementary approaches are
40 needed to quantify multiple modifications across biological contexts and to assess their associations to
41 transcriptional versus posttranscriptional events.

42 Tandem mass spectrometry (LC-MS/MS) is a highly accurate tool for analysis of modified
43 RNAs, which has so far been applied primarily in two approaches to identify and quantify RNA
44 modifications (21). The first approach employs LC-MS/MS of intact RNA oligonucleotides to detect
45 multiple modifications with positional information in specific RNA sequences. This approach is
46 chromatographically challenging (22) and requires advanced data mining for unambiguous
47 identification of RNA fragments, and it has so far been applied for comprehensive characterisation of
48 RNA modifications in abundant or short RNAs (22), such as rRNA (23–26), tRNAs (27, 28) and
49 miRNAs (29). The second approach employs LC-MS/MS of ribonucleosides for sensitive quantification
50 of RNA modifications (21). This approach, often combined with stable isotopes, can simultaneously
51 quantify the abundance of multiple modifications in specific RNA classes of interest, being highly

52 suitable to assess the presence of tRNA and rRNA modifications and their dynamics under various
53 biological scenarios (19, 27, 30–35). These methods have so far been applied mainly to study these
54 abundant RNA species because MS detection of mRNA modifications is unreliable due to the heavily
55 modified ncRNAs, which invariably contaminate mRNA pools purified using either polyA+-
56 enrichment or rRNA depletion (36, 37). Therefore, MS approaches are needed that are capable to
57 account for and quantitatively resolve the origin of multiple RNA modifications in purified RNA.
58 Moreover, the dynamic behavior of RNA modifications is insufficiently explained solely by changes in
59 their abundance (or levels), as these do not inform on the underlying pathways driving these changes.
60 Since the deposition (and removal) of RNA modifications is linked to the lifecycle of the RNAs
61 themselves (38–40), the change in methylation levels can result from changes either in RNA
62 (de)methylation rates and/or in the transcription or decay of methylated RNAs, From this lens, methods
63 are needed that can assess transcriptional and post-transcriptional effects on methylated RNAs under
64 non-stationary conditions.

65 Stable isotope labeling is a well-established method to quantify metabolic activity in cultured
66 cells (41–43). Here, we developed a quantitative approach using [¹³C-methyl]-methionine labeling and
67 mass spectrometry (MS) to assess the turnover of base modifications (¹³C-dynamods) in newly
68 transcribed RNA. With ¹³C-dynamods, we trace the proportion of newly methylated ribonucleosides
69 and their decay through time, i.e. methylation turnover, from digested polyadenylated RNA and
70 ncRNA. We first showed that polyadenylated RNA and ncRNA were distinguished by the different
71 turnover frequencies (in hr⁻¹) of modified ribonucleosides, which are inherently linked to the different
72 half-lives of mRNA, rRNA and tRNA (39, 44, 45). Examining the kinetics of methylation turnover at
73 steady-state within and across RNA classes as well as in free ribonucleosides enabled us to resolve the
74 origin of RNA modifications in digested RNA, and thereby uncover the presence of modifications in
75 uncharacterized RNA classes, such as *N*6,*N*6-dimethyladenosine (m⁶₂A). We then applied ¹³C-
76 dynamods in conjugation with abundance measurements of modified ribonucleosides in polyA+ and
77 ncRNA, which resolved their transcriptional versus posttranscriptional sensitivity in response to
78 actinomycin D and metabolic stresses. Thus, the quantitative nature of ¹³C-dynamods demonstrates its

79 capacity for sensitive characterization of modified ribonucleosides, their origin and dynamics, in
80 multiple RNA classes of interest.

81

RESULTS

82 ¹³C labeling of polyadenylated and ribosomal RNA modifications

83 S-adenosylmethionine (SAM) is the direct substrate of RNA methylation reactions in eukaryotic cells
84 (46). To trace the incorporation of SAM into RNA, we cultured 786O cells in methionine-free DMEM
85 medium supplemented with either unlabeled methionine ('Unlab') or [¹³C-methyl]-methionine, and
86 analyzed the isotopologues (m+0, m+1, m+2) of modified and unmodified ribonucleosides by tandem
87 mass spectrometry (LC-MS/MS) (Fig. 1A, 1B). The m+0 isotopologue (e.g. 150.1 *m/z* for m⁶A)
88 represents the mass of the analyzed molecule where all atoms are present as the most common isotope,
89 whereas the m+1 isotopologue (e.g. 151.1 *m/z* for m⁶A) indicates the mass shift due to ¹³C incorporation
90 from the ¹³C-labelled methionine tracer or from the natural abundance of ¹³C, ¹⁵N, ¹⁸O and ²H stable
91 isotopes. With ¹³C-dynamods, we measure the isotopologue fractions [m+1 / (m+1 + m+0)] of modified
92 and unmodified ribonucleosides, which reflect the amount of ¹³C enrichment (m+1) in the measured
93 ribonucleoside relative to the total pool of that ribonucleoside (m+1 + m+0) (Fig. 1A). Thus, the
94 isotopologue fractions of each ribonucleoside during [¹³C-methyl]-methionine labeling are internally
95 controlled for the amount of pre-existing ribonucleosides (m+0 and naturally labelled m+1) prior to ¹³C
96 labeling. Here, we analyzed the isotopologues of N⁶-methyladenosine (m⁶A), 7-methylguanosine
97 (m⁷G), 1-methyladenosine (m¹A), N⁶,N⁶-dimethyladenosine (m⁶₂A), 2'-O-methyladenosine (A_m), 5-
98 methylcytosine (m⁵C) and unmodified ribonucleosides from digested polyadenylated (polyA+), large
99 (>200 nt) and small (<200 nt) RNA. We observed increased m+1 and concomitant decreased m+0 ion
100 counts in modified ribonucleosides from polyA+ and large RNA after 4 and 24 hours of [¹³C-methyl]-
101 methionine labeling, while the m+1 fractions (natural abundance) of the unmodified ribonucleosides
102 was unaltered during the labeling period (Fig. 1C, 1D; fig. S1A; Supplementary Materials). We
103 determined that the ¹³C enrichment of intracellular methionine and SAM reaches a 98-100% plateau
104 within 30 minutes and remains constant thereafter (fig. S1B). Thus, the change in the 'heavy' (m+1)
105 isotopologue fraction relative to the unlabelled condition (natural abundance) indicates SAM-dependent
106 RNA methylation of newly synthesized RNA, whose turnover we have examined within and across
107 RNA classes. In contrast to singly methylated ribonucleosides, the m⁶₂A modification exhibited an

108 enrichment mostly of the m+2 isotopologue upon ^{13}C labeling (Fig. S1A), and so the m+2 fraction was
109 used to assess m^6A dynamics in subsequent analyses.

110 Quantification of isotopologue fractions showed a faster kinetics for m^6A , m^7G and m^5C in
111 polyA+ RNAs when compared to large RNA (>200nt) and small RNAs (<200 nt) (Fig. 1E), in
112 accordance with the faster lifecycle of mRNA in mammalian cells (45). In contrast, the kinetics of m^1A ,
113 m^6A and Am methylation was similar between polyA+ and large RNA fractions (Fig. 1E), suggesting
114 that a large portion of the signal for these modifications in the polyA+ fraction might derive from
115 contaminating ribosomal RNA (rRNA). Of note, the isotopologues are analyzed on all ribonucleosides
116 from the same polyA+ pool (Fig. S1C), so the purity of polyA+ enrichment is the same in all cases.
117 This indicates that the relative abundance in mRNAs vs contaminating ncRNA is much higher for m^6A ,
118 m^7G and m^5C compared to m^1A , m^6A and Am. Interestingly, we detected m^6A in small RNAs from
119 786O cells, and its kinetics was different when compared to large RNA (Fig. 1E).

120 **Methylation turnover to resolve the origin of RNA modifications and their presence in** 121 **uncharacterised RNA classes**

122 To examine the kinetics of methylation turnover, we cultured cells for 24 hours with [^{13}C -
123 methyl]-methionine followed by replacement (chase) with naturally labelled methionine and analyzed
124 the isotopologues over time. In accordance with the preceding findings (Fig. 1E), we observed an
125 exponential decay of the m+1 isotopologue fraction for $\text{m}^6\text{A}/\text{m}^7\text{G}$ but not for Am/ $\text{m}^1\text{A}/\text{m}^6\text{A}$ in polyA+
126 RNA (Fig. 2A). Conversely, the modifications of total/large RNAs exhibited uniformly slow turnover
127 (Fig. 2B), consistent with the high stability of rRNA and tRNA in growing cells (44). To test the kinetic
128 behavior underlying methylation turnover, we examined the goodness-of-fit of a linear versus
129 exponential regression of the isotopologue fraction. Analysis of residual errors showed that the linear
130 regression ($m_{(t)} = m_{(0)} + kt$) fits well the turnover of $\text{m}^1\text{A}/\text{m}^6\text{A}/\text{A}_m$ but not $\text{m}^6\text{A}/\text{m}^7\text{G}$ in polyA+ RNA,
131 in which the ‘U-shaped’ curve supports a non-linear model ($m_{(t)} = m_{(0)} e^{-kt}$) (Fig. 2C; fig. S2A).
132 Conversely, the linear regression fitted well the turnover of ncRNA modifications (fig. S2B, S2C). The
133 turnover frequency determined for Am/ $\text{m}^1\text{A}/\text{m}^6\text{A}$ in polyA+ was similar to ncRNA modifications ($k =$

134 0.031 hr⁻¹ on average), and significantly slower than m⁶A (k = 0.244 hr⁻¹) or m⁷G (k = 0.089 hr⁻¹) in
135 polyA⁺ RNA (Fig. 2A, 2B). Thus, the turnover of m¹A/m⁶₂A/A_m from polyA⁺ fractions is incompatible
136 with the exponential turnover of mRNA modifications (44, 45), confirming that they originate from
137 ncRNA contamination.

138 The m⁷G modification was similar to less abundant than m¹A/A_m/m⁶₂A in polyA⁺ RNA (Fig.
139 2D), and the sensitivity of MS detection was similar between m⁷G and m¹A/A_m/m⁶₂A, as determined
140 from equimolar injections of pure compounds (fig. S2D). Thus, the distinct turnover of RNA
141 modifications in the polyA⁺-purified fraction was not explained by analytical sensitivity or normalised
142 abundances alone. Instead, the modified ribonucleosides were more abundant in large RNA relative to
143 polyA⁺ RNA by a factor of 17/37/97/9 for A_m/m¹A/m⁶₂A/m⁷G, respectively, while m⁶A level was
144 greater in polyA⁺ RNA by a factor of 2 (Fig. 2E). From the determined turnover frequencies (hr⁻¹) of
145 ncRNA (Fig. 2B), we estimated that a 50% contribution of ncRNA signal to the ribonucleoside pool in
146 polyA⁺-purified RNA would lower the detected turnover of the bona fide m⁶A mRNA modification,
147 with a turnover frequency of 0.242hr⁻¹, to that of m⁷G, with a turnover frequency of ~0.09 hr⁻¹ (fig.
148 S2E). That is, reliable turnover-based detection of a hypothetical mRNA modification that is more
149 abundant by a factor of 17-97 in ncRNA relative to mRNA is attainable with a maximal ncRNA
150 contamination of 0.5% (50%/97) to 2.9% (50%/17), but even an optimal performance of available
151 methods to purify polyA⁺ RNA commonly contains 2-3% of contaminating ncRNA (fig. S2F) (36, 37).
152 Thus, the ability to resolve bona fide mRNA modifications based on methylation turnover is limited by
153 the depletion efficiency of highly abundant rRNA modifications.

154 As the turnover frequency of m⁶A was ~8 times faster in polyA⁺ RNA than ncRNA (Fig 2A,
155 2B), we reasoned that free ribonucleosides derived from metabolic extracts would be derived mainly
156 from endogenous degradation of mRNAs, rather than ncRNAs. Thus, we employed ¹³C-dynamods to
157 examine the methylation turnover of free ribonucleosides, thereby enriching for mRNA-derived
158 ribonucleosides and decreasing interference from rRNA-derived ribonucleosides. We found a fast
159 kinetics following ¹³C labeling that was similar for m⁶A, m⁷G and A_m, indicating that they are primarily
160 derived from the same RNA type (i.e. mRNAs) (Fig. 2F, 2G, 2H). Interestingly, the m⁶₂A modification

161 also exhibited a non-linear, faster kinetics than m¹A or 1-methylguanosine (m¹G) (Fig. 2F, 2G, 2H),
162 which are known tRNA modifications and were present in the metabolic extracts at high levels (fig.
163 S2G) (47). We did not include the isotopologue analysis of m⁵C in the time-series experiments due to
164 low abundance of its free ribonucleosides, and due to low MS sensitivity for m⁵C (Fig. 2D; fig. S2D,
165 S2G), which compromises the quantification under conditions of partial ¹³C labeling. Thus, while the
166 turnover analysis of the polyA+ fraction couldn't be used to validate lowly abundant modifications due
167 to rRNA contamination (Fig. 2E), the turnover of Am and m⁶₂A in the free pool suggests that these
168 modifications indeed partly derive from rapidly decaying, non-ribosomal RNAs (Fig 2F), which may
169 include mRNAs. This was supported by the normalized levels of A_m and m⁶₂A in the free pool being
170 more similar to those of polyA+ than rRNA (fig. S2H). These results confirm the presence of A_m in
171 mRNA (48) and suggest m⁶₂A is more common in short-lived RNAs than m¹A, which has already been
172 studied in mRNAs (49, 50).

173 **Sensitivity of RNA modifications to metabolic stresses**

174 The maintenance of methylation reactions requires SAM and serine/glycine, which feed one-
175 carbon metabolism and SAM synthesis (51). Conversely, RNA demethylation is catalysed by α -
176 ketoglutarate (α -kg)-dependent dioxygenases such as FTO and ALKBH5, which act on m⁶A, N⁶,2-*O*-
177 dimethyladenosine (m⁶A_m) and m¹A (52, 53). We measured both the methylation turnover and
178 abundance of modified ribonucleosides to obtain insights into the sensitivity of mRNA versus ncRNA
179 to metabolic stresses linked to RNA (de)methylation. First, we confirmed that actinomycin (ActD), a
180 pan inhibitor of eukaryotic transcription, completely inhibited the methylation turnover of polyA+ and
181 large RNA (Fig. 3A), in accordance with the co-transcriptional deposition of mRNA and most rRNA
182 modifications (54–57). Treatment with ActD decreased the normalised levels of m⁶A (m⁶A/A) in
183 polyA+ RNA (Fig. 3B), but not of m⁷G, which supports the role of m⁶A in global mRNA destabilisation,
184 as initially reported (40). Deprivation of serine or glutamine inhibited mainly the methylation turnover
185 of large RNA (Fig. 3C, 3D). In contrast, the abundance of modified ribonucleosides in large RNA was
186 unaltered under these forms of stress (Fig. 3E) whereas glutamine deprivation led to increased m⁶A
187 levels in polyA+ RNA (Fig. 3F), which was in contrast to ActD treatment (Fig. 3B). Thus, the reduced

188 methylation turnover of large RNA simply results from an inhibited transcription of the rRNAs
189 themselves, while the altered abundance of m⁶A without significant changes in its turnover indicates its
190 post-transcriptional lability to stress conditions via altered i) decay of m⁶A-enriched vs. m⁶A-depleted
191 mRNAs or ii) dynamics of the m⁶A modification itself. These data show that measurements of
192 methylation turnover and ribonucleoside abundances resolve transcriptional versus post-transcriptional
193 effects on RNA modifications in non-stationary (stimulus-dependent) experiments.

194

DISCUSSION

195 Isotopic labeling of cultured cells is a well-established method to quantify metabolic activity,
196 but its application to RNA modifications has been limited to ncRNAs (33, 58). Here, we demonstrate
197 that quantification of methylation turnover with dynamic ¹³C labeling informs on the distinct dynamics
198 of polyA+ and ncRNA modifications, and their sensitivity to metabolic perturbations of mammalian
199 cells. ¹³C-dynamods presents several advances in the application of mass spectrometry (MS) approaches
200 to study RNA turnover & dynamics. First, in contrast to approaches that rely on prior/in-parallel labeling
201 with ¹⁵N/¹³C-enriched nucleosides to distinguish between pre-existing and newly modified RNA (33,
202 58), the ‘heavy’ isotopologue fraction derived from [¹³C-methyl]-methionine is internally controlled for
203 the amount of unlabelled, pre-existing ribonucleosides, and is thus specific to modified ribonucleosides.
204 Second, in contrast to approaches using multiplexing or spiking from isotopically labelled cultures (24,
205 25, 32, 58), the dynamic ¹³C labeling over time directly informs on the turnover frequency (in hr⁻¹) (41,
206 43) of various RNA modifications, as the direct substrate (SAM) of the targeted reaction (RNA
207 methylation) is close to 100% labelled in less than 30 minutes in cell culture (fig. S1B) (43). Moreover,
208 SAM needs not be fully labelled for comparisons of dynamic ¹³C labeling between modifications at
209 early, single time points as its ¹³C enrichment is expected to be equal across SAM-dependent RNA
210 modifications. Third, conventional RNA labeling approaches using ribonucleoside analogues or
211 precursors rely on their incorporation into newly synthesized RNA through the salvage pathway (e.g.
212 uridine and its analogs) (45, 59) or the *de novo* pathway (glucose, serine/glycine or water tracers) of
213 ribonucleotide (NTP) synthesis (60–64). In contrast, the methylation of newly transcribed RNA occurs
214 downstream (co-transcriptionally) of NTP synthesis, making it a reliable readout of RNA turnover,

215 particularly under non-stationary conditions that may alter the relative activity of NTP synthesis
216 pathways (65, 66). Also, the nucleotide recycling through the salvage pathway may lead to ineffective
217 ‘washout’ with unlabelled nucleotides in chase experiments (59, 66), whereas a new SAM molecule is
218 used in each (co-transcriptional) methylation cycle in ^{13}C -dynamods, adding to the specificity and
219 versatility of experimental designs (59). Finally, combined measurements of methylation turnover and
220 ribonucleoside levels allow ^{13}C -dynamods to also inform on transcriptional versus posttranscriptional
221 sensitivity of RNA modifications in response to a stimulus.

222 Reliable study of mRNA modifications by MS analyses of ribonucleosides is challenging due
223 to the high abundance of heavily modified ncRNAs that invariably contaminate the polyA+ fraction
224 (36, 37). To address this challenge, we exploited the fact that the lifecycle of methylated RNA follows
225 the lifecycle of the RNAs at metabolic steady-state (38–40). The decay of mRNA is fast with a median
226 half-life from 40 min to 9 hours in mammalian cells (44, 67, 68), while rRNA and tRNA exhibit half-
227 lives of 60-70 hours in growing fibroblasts (44). By definition, the methylation turnover as determined
228 by ^{13}C incorporation into newly methylated RNA does not assess non-modified RNAs, and hence does
229 not capture the removal of RNA modifications. That is, any RNA demethylation activity can only affect
230 the abundances of modified ribonucleosides as a whole (sum of m+1 and m+1), not the m+1 or m+0
231 isotopologues individually, which would be required to cause a differential m+1 fraction. Since RNA
232 transcription and decay rates are constant at metabolic steady-state, we propose that the methylation
233 turnover is an accurate readout of RNA turnover, which allowed us to assess the contributions of short-
234 lived (mRNAs) and long-lived (non-coding) RNAs to a pool of modified RNAs and free
235 ribonucleosides. Indeed, this information could not be drawn if labelled ribonucleoside themselves or
236 its precursors were used to trace ribonucleotide synthesis (via the salvage and *de novo* pathways) or
237 transcription. Likewise, the source RNA cannot be pinpointed if the abundance (levels) of modified
238 ribonucleosides measured in isolation.

239 Using this approach, we could not reliably determine highly abundant rRNA modifications
240 ($\text{Am}/\text{m}^1\text{A}/\text{m}^6_2\text{A}$) in polyA+-purified RNA as being derived from mRNAs. Based on methylation
241 turnover, we estimated that these modifications in the polyA+ fraction could be detected with a maximal

242 ncRNA contamination of 0.5-2.9%, since Am/m¹A/m⁶₂A levels were found higher in ncRNAs by a
243 factor of 17-37-97, respectively. In contrast, a ~6% of ncRNA contamination would be required to fully
244 account for the slower m⁷G turnover detected in polyA⁺ RNA, since m⁷G levels were found only ~9
245 times higher in ncRNAs. As the m⁷G turnover reflected that of a bona fide mRNA modification, its
246 slower kinetics in polyA⁺-purified RNA suggests a temporal delay relative to m⁶A turnover. A further
247 evidence for the distinct turnover of m⁷G relative to m⁶A in mRNAs is the response to metabolic
248 stresses, where the m⁷G turnover changed in large RNA but not polyA⁺ RNA following 4 hours of ¹³C
249 labeling (Fig. 3c, 3d). In this respect, while m⁶A is co-transcriptionally deposited in mRNA (39, 54,
250 56), m⁷G is an essential modification at the 5' cap of mRNA that can be placed both in the nucleus and
251 cytoplasm (69, 70). Moreover, m⁷G sites have been reported internally within mRNA, catalysed by the
252 cytosolic METTL1 methyltransferase (71). Taken together, the distinct kinetics of m⁷G and m⁶A in
253 polyadenylated RNA suggest compartmentalization differences affecting their temporal deposition into
254 newly synthesized mRNA.

255 Previous reports identified m⁵C and Am as mRNA modifications (48, 72), and more recently
256 also m¹A (49, 50). Our analysis of free ribonucleosides showed a similarly fast kinetics for the turnover
257 of Am, m⁶A and m⁷G, consistent with these modifications being derived from the rapidly decaying
258 mRNAs. This was supported by the normalized levels of free modified ribonucleosides being more
259 similar to those of polyA⁺-purified than of ncRNAs. In contrast, the turnover of free m¹A and m¹G
260 ribonucleosides was significantly slower, indicating that these modifications are predominantly derived
261 from a ncRNA class, likely tRNAs, where they are present at high levels (47). This aligns with the
262 recent conclusions that m¹A might be restricted to a handful of mRNAs (3, 49). Finally, despite the low
263 sensitivity of m⁵C detection in chase experiments, the quantification of m⁵C isotopologues at 24 hours
264 is consistent with it being derived from mRNA (72).

265 The m⁶₂A modification is thought to be present primarily in the 18S and 12S rRNA of
266 mammalian transcriptomes (26, 73, 74). While m⁶₂A has been detected in bacterial tRNA (75), care
267 must be taken with abundant m⁶₂A-modified rRNA fragments that co-purify with tRNA (76), and are
268 not resolved by standard MS quantifications. Here, we detected slower turnover of m⁶₂A in mammalian

269 small RNAs relative to large RNA, raising the possibility that this modification is present in non-
270 18S/12S RNA species, e.g. in small rRNA and/or tRNAs. Nevertheless, an unlikely possibility from
271 ¹³C-dynamods measurements remains that m⁶A-containing 18S/12S rRNA fragments are turned over
272 at a slower rate than m⁶A-containing intact rRNAs. Interestingly, the turnover of free m⁶A
273 ribonucleosides exhibited a faster kinetics than free m¹A/m¹G (canonical ncRNA modifications) (47)
274 and when compared to large RNA modifications, suggesting that m⁶A is also present in RNAs of high
275 turnover RNAs, which likely include mRNAs and short-lived ncRNAs. The presence and role of m⁶A
276 beyond the 18S/12S rRNAs thus merits further investigation. Of note, single methylation intermediates
277 of m⁶A have been detected *in vitro* (77), but we did not detect m+1 isotopologues for m⁶A above its
278 natural abundance. As SAM was 98-100% ¹³C-labelled within 30 minutes, the time resolution of our
279 experiments does not capture sequential methylation of adenosine into m⁶A. These various findings
280 highlight the value examining the turnover of methylated RNA to uncover the presence of modifications
281 in uncharacterised in RNA subclasses, which warrants further investigation.

282 A non-stationary condition, e.g. a stress condition, may affect the afferent (i.e. methylation of
283 newly transcribed RNA) or efferent (i.e. decay of methylated RNAs) turnover parts of methylated
284 RNAs. Combined with abundance measurements, this allowed us to assess transcriptional versus non-
285 transcriptional sensitivity of modified RNAs to stress conditions. This was evidenced by the reduced
286 methylation turnover of ncRNAs following serine deprivation and ActD treatment, wherein the
287 abundance of modifications was unaltered in the former (transcriptional effect) but m⁶A levels
288 decreased in the latter (posttranscriptional effect). The observed inhibited turnover of methylated
289 ncRNAs under serine deprivation is in line with the expected inhibition of mTOR activity, and thereby
290 of rRNA biogenesis (78). In contrast to ncRNAs, glutamine deprivation increased m⁶A levels in
291 polyA+-purified RNA without significantly changing (not increasing) its turnover. These data suggest
292 that m⁶A is post-transcriptionally sensitive to glutamine levels through either i) an altered decay of
293 m⁶A-enriched vs. m⁶A-depleted RNAs, or ii) inhibition of m⁶A demethylation itself. The demethylation
294 of m⁶A is a step-wise conversion into adenosine through the formation of N6-hydroxymethyladenosine
295 (hm⁶A) and N6-formyladenosine (f⁶A) intermediates (79), whose presence or turnover was not assessed.

296 Thus, related developments are needed to address if post-transcriptional dynamics of m⁶A by metabolic
297 stress conditions are due to RNA demethylation or differential decay of m⁶A-modified versus m⁶A-
298 depleted unmodified RNAs. As glutamine is the main carbon source of α -ketoglutarate, a co-substrate
299 of RNA demethylases (52, 53), it is plausible that its depletion could inhibit RNA demethylation. This
300 supports the notion that the reversibility of m⁶A in mRNA is likely context-dependent (80). With
301 exception of ActD treatment, the stimuli examined did not lead to changes in both the turnover and
302 abundances of modified ribonucleosides. In this respect, while altered methylation turnover (and
303 unaltered abundance) indicates a transcriptional effect, it is plausible that a stimulus may alter
304 methylation turnover at the post-transcriptional level e.g. if the newly methylated (m+1 fraction) and
305 pre-existing methylated (m+0 fraction) RNAs differently are exposed differently to RNA degradation,
306 e.g. through nuclear/cytosolic compartmentalisation.

307 Our study demonstrates how quantification of methylation turnover and abundance can be used
308 to examine the presence of RNA modifications in RNA classes, their temporal dynamics and sensitivity
309 to metabolic stress conditions. These insights open new directions to be further explored by MS and
310 orthogonal approaches to obtain information on particular RNAs.

311

312

AUTHOR CONTRIBUTIONS

313 Paulo A. Gameiro: Conceptualization, Methodology, Formal analysis, Investigation, Resources, Data
314 curation, Original Draft, Writing – Original Draft, Writing – Review & Editing, Visualization, Funding
315 acquisition; Vesela Encheva: Methodology, Formal analysis; Mariana Silva Dos Santos: Formal
316 analysis; James I MacRae: Resources, Writing – Review & Editing, Funding acquisition; Jernej Ule:
317 Resources, Writing – Original Draft, Writing – Review & Editing, Supervision, Funding acquisition.

318

ACKNOWLEDGMENTS

319 This project has received funding from Wellcome Trust (103760/Z/14/Z) and the European Research
320 Council (ERC) under the European Union's Seventh Framework Program (FP7/2007-2013)/ERC grant
321 agreement ID: 617837). P.A.G was supported by a Marie Skłodowska-Curie individual fellowship

322 (grant agreement ID: 701730). The Francis Crick Institute receives its core funding from Cancer
323 Research UK (grant no. FC001002), the UK Medical Research Council (grant no. FC001002) and the
324 Wellcome Trust (grant no. FC001002).

325 **CONFLICTS OF INTEREST**

326 The authors declare that they have no competing interests.

327 **EXPERIMENTAL PROCEDURES**

328 **Cell culture and metabolic labeling.** 786O cells were obtained from the Crick Cell Services and
329 cultured at 37°C with 5% CO₂ in high glucose DMEM medium (ThermoFisher Scientific, #61965026)
330 supplemented with 10% fetal bovine serum (FBS) (ThermoFisher Scientific, #21875034). For ¹³C
331 labeling experiments, 786O cells were grown in high glucose DMEM medium without glutamine,
332 methionine and cystine (ThermoFisher Scientific, #21013024) supplemented with 10% dialyzed FBS
333 (ThermoFisher Scientific, #26400044), 2 mM glutamine, 0.1 mM cystine and 0.2 mM [¹³C-methyl]-
334 methionine (CK Isotopes Limited). Cells were maintained at 50-60% confluence (or 30-40% in chase
335 experiments) and washed with PBS before switching to ¹³C-labelled medium (or regular medium in
336 chase) for the indicated time periods.

337 **RNA purification.** At the conclusion of metabolic labeling, the medium was aspirated and extraction
338 of total RNA was performed with the mirVana isolation kit according to manufacturer's instructions
339 (Thermofisher Scientific, #AM1560). Large (>200nt) RNAs were purified by adding 1/3 volume of
340 100% ethanol to the aqueous phase recovered from the organic extraction before loading into the filter
341 cartridge of the mirVana Kit. Small (<200nt) RNAs were purified by collecting the total filtrate, addition
342 of 2/3 volume of 100% ethanol and loading into the filter cartridge. Polyadenylated RNA was purified
343 from total/large RNA via two rounds of polyA tail hybridization with Oligo-dT magnetic Dynabeads
344 (ThermoFisher Scientific, #61002).

345 **LC-MS/MS analysis of ribonucleosides.** Purified RNA (100-250 ng) was digested into
346 ribonucleosides using one unit of nuclease P1 (Sigma-Aldrich, #N8630-1VL) in 25 µl of buffer 25 mM

347 NaCl, 2.5 mM ZnCl₂ and 10mM NaCH₃COO pH 5.3 and incubated for 2 hours at 37°C. Subsequently,
348 NH₄HCO₃ (100 mM) and 5 units of alkaline phosphatase (CIP) (NEB, #M0525S) were added and the
349 sample incubated for 2 hours (or 20 min, with Quick CIP) at 37°C. Formic acid was added at 0.1% v/v
350 in a final volume of 50 µl and samples were filtered (0.22 µm, Millipore) and 15-20 µl analyzed in
351 duplicate by LC-MS. Ribonucleosides were resolved with a C18 reverse phase column (100 x 2.1 mm,
352 3 µm particle size, Chromex Scientific, #F18-020503) and eluted with a gradient of 0.1% v/v formic
353 acid (solvent A) and 80% acetonitrile in 0.1% formic acid (solvent B) at a flow rate of 0.2 ml/min and
354 40°C: 100% solvent A for 3 min, 12% solvent B for 12 min, and 100% solvent B for 2 min after which
355 the column was re-equilibrated with 100% solvent A for 3 min (20 min total run time). The
356 ribonucleoside separation was performed using U3000 HPLC (Thermo Scientific) and the detection by
357 a TSQ Quantiva Triple Quadrupole mass spectrometer (TSQ Quantiva, Thermo Scientific) controlled
358 by the Xcalibur software version 4.0.27 (Thermo Scientific). The HPLC was coupled to the TSQ
359 Quantiva using a HESI (heated electrospray) ion source (Thermo Scientific) operating in positive
360 ionization mode with the following parameters: capillary voltage, 3500V; sheath gas flow, 7.35 l/min;
361 gas temperature, 325C. The first and third quadrupoles (Q1 and Q3) were stringently fixed to 0.2 units
362 of resolution and set to detect the mass of the precursor ribonucleoside ion (Q1) and of the base and
363 ribose product ions (Q3). The ribonucleosides were identified by comparison of the retention time and
364 detected mass transitions to commercially available standards. The collision energies were
365 experimentally defined based on the fragmentation pattern of each ribonucleoside standard and chosen
366 based on the maximum intensity of the base product; the ribose ring was used only as a qualifying
367 transition. The retention time, mass transitions (*m/z*) and collision energies of each ribonucleoside were:
368 adenosine, ~4.1 min, 268.1 → 136.1 *m/z*, 20 V; guanosine, ~5.4 min, 284.1 → 135.0 *m/z*, 35.5 V;
369 cytidine, ~1.4 min, 244.2 → 112.05 *m/z*, 12 V; m⁶A, ~8.7 min, 282.1 → 150.1 *m/z*, 20 V; m¹A, ~1.8
370 min, 282.1 → 150.1 *m/z*, 20V, m⁷G, ~2.3 min, 298.05 → 166.1 *m/z*, 20V; m⁵C, ~1.8 min, 258.2 →
371 126.1, *m/z*, 13V; m⁶₂A, ~11.9 min, 296.2 → 164.1 *m/z*, 22V. Each mass transition above corresponded
372 to the m+0 isotopologue, and increased by one (m+1), two (m+2) and three (m+3) units for detection
373 of the other isotopologues *e.g.* m⁶₂A: 297.2 → 165.1 (m+1), 298.2 → 166.1 (m+2), 299.2 → 167.1
374 (m+3). The dwell time for each transition was 30 ms for a duty cycle of 930 ms (31 transitions), and 8

375 to 20 data points per chromatographic peak were obtained for ‘short’ and ‘long’ peaks, respectively. A
376 mix of ribonucleoside standards containing 0.5, 1, 5, 10, 50, 100, 500 fmol, 1, 5, 10, 50 or 100 pmol of
377 each ribonucleoside was run in parallel after the biological samples for absolute quantifications, a subset
378 of which is shown in Extended Data Fig. 2d. Data were recorded using the Xcalibur 3.0.63 software
379 (ThermoFisher Scientific) and analyzed using Skyline (version 19.1) (81) (Supplementary Materials).

380 **Metabolite extraction and LC-MS analysis of SAM/free ribonucleosides.** At the end of cell culture
381 with [¹³C-methyl]-methionine, metabolic activity quenched by adding ice-cold PBS. Metabolites were
382 extracted by addition of 600 µl ice-cold 1:1 (vol/vol) methanol/water to the cell pellets, samples were
383 transferred to a chilled microcentrifuge tube containing 300µl chloroform and 600µl methanol (1500 µl
384 total, in 3:1:1 vol/vol methanol/water/chloroform). Samples were sonicated in a water bath for 8 min at
385 4°C, and centrifuged (13000 rpm) for 10 min at 4°C. The supernatant containing the extract was
386 transferred to a new tube for evaporation in a speed-vacuum centrifuge, resuspended in 3:3:1
387 (vol/vol/vol) methanol/water/chloroform (350µl total) to phase separate polar metabolites (upper
388 aqueous phase) from non-polar metabolites (lower organic phase), and centrifuged. The aqueous phase
389 was transferred to a new tube for evaporation in a speed-vacuum centrifuge, and resuspended in 100µl
390 water for LC-MS acquisition. LC-MS analysis was performed using a Dionex UltiMate LC system
391 (ThermoFisher Scientific) with a ZIC-pHILIC column (150 mm x 4.6 mm, 5 µm particle, Merck
392 Sequant), as described previously (82). A 15 min elution gradient of 80% Solvent A (20 mM ammonium
393 carbonate in Optima HPLC grade water, Sigma Aldrich) to 20% Solvent B (acetonitrile Optima HPLC
394 grade, Sigma Aldrich) was used, followed by a 5 min wash of 95:5 Solvent A to Solvent B and 5 min
395 re-equilibration. Other parameters were as follows: flow rate, 300 µL/min; column temperature, 25°C;
396 injection volume, 10 µL; autosampler temperature, 4°C. All metabolites were detected across a mass
397 range of 70-1050 *m/z* using a Q Exactive Orbitrap instrument (ThermoFisher Scientific) with heated
398 electrospray ionization and polarity switching mode at a resolution of 70,000 (at 200 *m/z*). MS
399 parameters were as follows: spray voltage 3.5 kV for positive mode and 3.2 kV for negative mode;
400 probe temperature, 320°C; sheath gas, 30 arbitrary units; auxiliary gas, 5 arbitrary units. Parallel
401 reaction monitoring (PRM) was used at a resolution of 17,500 to confirm the identification of

402 metabolites; collision energies were set individually in HCD (high-energy collisional dissociation)
403 mode. Data were recorded using the Xcalibur 3.0.63 software and analyzed using Tracefinder 4.1
404 (ThermoFisher Scientific) according to the manufacturer's workflows.

405 **Quantification of methylation turnover.** The isotopologue fractions were defined as the total ion
406 counts of the m+1 isotopologue (except for m+2 in m⁶₂A) relative to the total ion counts of the m+0
407 plus m+1 isotopologues. The kinetics of isotopologue fractions and goodness-of-fit were determined
408 using the Curve Fitting toolbox of Matlab R2020a (MathWorks) either by a linear regression [$f(x) =$
409 $p_1 \cdot x + p_2$] or an exponential fit: a one-term function in the chase experiments [$f(x) = a \cdot \exp(b \cdot x)$,
410 Levenberg-Marquardt algorithm] and a two-term function to fit the isotopologue fractions of free
411 ribonucleosides [$f(x) = a \cdot \exp(b \cdot x) + c \cdot \exp(d \cdot x)$, Levenberg-Marquardt algorithm].

REFERENCES

- 413 1. Capitanichik, C., Toolan-Kerr, P., Luscombe, N. M., and Ule, J. (2020) How Do You Identify
414 m6 A Methylation in Transcriptomes at High Resolution? A Comparison of Recent Datasets.
415 *Front. Genet.* **11**, 398
- 416 2. Helm, M., and Motorin, Y. (2017) Detecting RNA modifications in the epitranscriptome:
417 predict and validate. *Nat. Rev. Genet.* **18**, 275–291
- 418 3. Grozhik, A. V., and Jaffrey, S. R. (2018) Distinguishing RNA modifications from noise in
419 epitranscriptome maps. *Nat. Chem. Biol.* **14**, 215–225
- 420 4. Roundtree, I. A., Evans, M. E., Pan, T., and He, C. (2017) Dynamic RNA Modifications in
421 Gene Expression Regulation. *Cell.* **169**, 1187–1200
- 422 5. Frye, M., Harada, B. T., Behm, M., and He, C. (2018) RNA modifications modulate gene
423 expression during development. *Science (80-.)*. **361**, 1346–1349
- 424 6. Batista, P. J., Molinie, B., Wang, J., Qu, K., Zhang, J., Li, L., Bouley, D. M., Lujan, E.,
425 Haddad, B., Daneshvar, K., Carter, A. C., Flynn, R. A., Zhou, C., Lim, K.-S., Dedon, P.,
426 Wernig, M., Mullen, A. C., Xing, Y., Giallourakis, C. C., and Chang, H. Y. (2014) m6A RNA
427 Modification Controls Cell Fate Transition in Mammalian Embryonic Stem Cells. *Cell Stem*
428 *Cell.* **15**, 707–719
- 429 7. Li, H.-B., Tong, J., Zhu, S., Batista, P. J., Duffy, E. E., Zhao, J., Bailis, W., Cao, G.,
430 Kroehling, L., Chen, Y., Wang, G., Broughton, J. P., Chen, Y. G., Kluger, Y., Simon, M. D.,
431 Chang, H. Y., Yin, Z., and Flavell, R. A. (2017) m6A mRNA methylation controls T cell
432 homeostasis by targeting the IL-7/STAT5/SOCS pathways. *Nature*. 10.1038/nature23450
- 433 8. Yoon, K. J., Ringeling, F. R., Vissers, C., Jacob, F., Pokrass, M., Jimenez-Cyrus, D., Su, Y.,
434 Kim, N. S., Zhu, Y., Zheng, L., Kim, S., Wang, X., Doré, L. C., Jin, P., Regot, S., Zhuang, X.,
435 Canzar, S., He, C., Ming, G. li, and Song, H. (2017) Temporal Control of Mammalian Cortical
436 Neurogenesis by m6A Methylation. *Cell*. 10.1016/j.cell.2017.09.003
- 437 9. Su, R., Dong, L., Li, C., Nachtergaele, S., Wunderlich, M., Qing, Y., Deng, X., Wang, Y.,
438 Weng, X., Hu, C., Yu, M., Skibbe, J., Dai, Q., Zou, D., Wu, T., Yu, K., Weng, H., Huang, H.,
439 Ferchen, K., Qin, X., Zhang, B., Qi, J., Sasaki, A. T., Plas, D. R., Bradner, J. E., Wei, M.,
440 Marcucci, G., Jiang, X., Mulloy, J. C., Jin, J., He, C., and Chen, J. (2017) R-2HG Exhibits
441 Anti-tumor Activity by Targeting FTO/m6A/MYC/CEBPA Signaling. *Cell.* **172**, 90-91.e23
- 442 10. Qing, Y., Dong, L., Gao, L., Li, C., Li, Y., Han, L., Prince, E., Tan, B., Deng, X., Wetzel, C.,
443 Shen, C., Gao, M., Chen, Z., Li, W., Zhang, B., Braas, D., ten Hoeve, J., Sanchez, G. J., Chen,
444 H., Chan, L. N., Chen, C.-W., Ann, D., Jiang, L., Müschen, M., Marcucci, G., Plas, D. R., Li,
445 Z., Su, R., and Chen, J. (2021) R-2-hydroxyglutarate attenuates aerobic glycolysis in leukemia
446 by targeting the FTO/m6A/PFKP/LDHB axis. *Mol. Cell*. 10.1016/j.molcel.2020.12.026
- 447 11. Min, K. W., Zealy, R. W., Davila, S., Fomin, M., Cummings, J. C., Makowsky, D., Mcdowell,
448 C. H., Thigpen, H., Hafner, M., Kwon, S. H., Georgescu, C., Wren, J. D., and Yoon, J. H.
449 (2018) Profiling of m6A RNA modifications identified an age-associated regulation of AGO2
450 mRNA stability. *Aging Cell*. 10.1111/accel.12753
- 451 12. Wu, Z., Shi, Y., Lu, M., Song, M., Yu, Z., Wang, J., Wang, S., Ren, J., Yang, Y. G., Liu, G.
452 H., Zhang, W., Ci, W., and Qu, J. (2020) METTL3 counteracts premature aging via m6A-
453 dependent stabilization of MIS12 mRNA. *Nucleic Acids Res.* **48**, 11083–11096
- 454 13. Livneh, I., Moshitch-Moshkovitz, S., Amariglio, N., Rechavi, G., and Dominianni, D. (2020)
455 The m6A epitranscriptome: transcriptome plasticity in brain development and function. *Nat.*
456 *Rev. Neurosci.* **21**, 36–51
- 457 14. Chen, X., Yu, C., Guo, M., Zheng, X., Ali, S., Huang, H., Zhang, L., Wang, S., Huang, Y.,
458 Qie, S., and Wang, J. (2019) Down-Regulation of m6A mRNA Methylation Is Involved in
459 Dopaminergic Neuronal Death. *ACS Chem. Neurosci.* **10**, 2355–2363
- 460 15. Han, M., Liu, Z., Xu, Y., Liu, X., Wang, D., Li, F., Wang, Y., and Bi, J. (2020) Abnormality
461 of m6A mRNA Methylation Is Involved in Alzheimer’s Disease. *Front. Neurosci.* **14**, 1–9
- 462 16. Schaefer, M., Pollex, T., Hanna, K., Tuorto, F., Meusburger, M., Helm, M., and Lyko, F.
463 (2010) RNA methylation by Dnmt2 protects transfer RNAs against stress-induced cleavage.
464 *Genes Dev.* **24**, 1590–5
- 465 17. Blanco, S., Dietmann, S., Flores, J. V., Hussain, S., Kutter, C., Humphreys, P., Lukk, M.,

- 466 Lombard, P., Treps, L., Popis, M., Kellner, S., Holter, S. M., Garrett, L., Wurst, W., Becker,
467 L., Klopstock, T., Fuchs, H., Gailus-Durner, V., Hrabe de Angelis, M., Karadottir, R. T.,
468 Helm, M., Ule, J., Gleeson, J. G., Odom, D. T., and Frye, M. (2014) Aberrant methylation of
469 tRNAs links cellular stress to neuro-developmental disorders. *EMBO J.* **33**, 2020–2039
- 470 18. Gkatza, N. A., Castro, C., Harvey, R. F., Heiß, M., Popis, M. C., Blanco, S., Bornelöv, S.,
471 Sajini, A. A., Gleeson, J. G., Griffin, J. L., West, J. A., Kellner, S., Willis, A. E., Dietmann, S.,
472 and Frye, M. (2019) *Cytosine-5 RNA methylation links protein synthesis to cell metabolism*,
473 10.1371/journal.pbio.3000297
- 474 19. Gu, C., Begley, T. J., and Dedon, P. C. (2014) tRNA modifications regulate translation during
475 cellular stress. *FEBS Lett.* **588**, 4287–4296
- 476 20. Lovén, J., Orlando, D. A., Sigova, A. A., Lin, C. Y., Rahl, P. B., Burge, C. B., Levens, D. L.,
477 Lee, T. I., and Young, R. A. (2012) Revisiting global gene expression analysis. *Cell.* **151**, 476–
478 482
- 479 21. Wetzel, C., and Limbach, P. A. (2016) Mass spectrometry of modified RNAs: Recent
480 developments. *Analyst.* **141**, 16–23
- 481 22. Huber, C. G., and Oberacher, H. (2001) Analysis of nucleic acids by on-line liquid
482 chromatography-mass spectrometry. *Mass Spectrom. Rev.* **20**, 310–343
- 483 23. Taoka, M., Nobe, Y., Hori, M., Takeuchi, A., Masaki, S., Yamauchi, Y., Nakayama, H.,
484 Takahashi, N., and Isobe, T. (2015) A mass spectrometry-based method for comprehensive
485 quantitative determination of post-transcriptional RNA modifications: The complete chemical
486 structure of *Schizosaccharomyces pombe* ribosomal RNAs. *Nucleic Acids Res.*
487 10.1093/nar/gkv560
- 488 24. Waghmare, S. P., and Dickman, M. J. (2011) Characterization and quantification of RNA post-
489 transcriptional modifications using stable isotope labeling of RNA in conjunction with mass
490 spectrometry analysis. *Anal. Chem.* **83**, 4894–4901
- 491 25. Popova, A. M., and Williamson, J. R. (2014) Quantitative Analysis of rRNA Modifications
492 Using Stable Isotope Labeling and Mass Spectrometry
- 493 26. Taoka, M., Nobe, Y., Yamaki, Y., Sato, K., Ishikawa, H., Izumikawa, K., Yamauchi, Y.,
494 Hirota, K., Nakayama, H., Takahashi, N., and Isobe, T. (2018) Landscape of the complete
495 RNA chemical modifications in the human 80S ribosome. *Nucleic Acids Res.*
496 10.1093/NAR/GKY811
- 497 27. Suzuki, T., and Suzuki, T. (2014) A complete landscape of post-transcriptional modifications
498 in mammalian mitochondrial tRNAs. *Nucleic Acids Res.* **42**, 7346–7357
- 499 28. Wein, S., Andrews, B., Sachsenberg, T., Santos-Rosa, H., Kohlbacher, O., Kouzarides, T.,
500 Garcia, B. A., and Weissner, H. (2020) A computational platform for high-throughput analysis
501 of RNA sequences and modifications by mass spectrometry. *Nat. Commun.* **11**, 926
- 502 29. Kullolli, M., Knouf, E., Arampatzidou, M., Tewari, M., and Pitteri, S. J. (2014) Intact
503 MicroRNA analysis using high resolution mass spectrometry. *J. Am. Soc. Mass Spectrom.* **25**,
504 80–87
- 505 30. Chan, C. T. Y., Dyavaiah, M., DeMott, M. S., Taghizadeh, K., Dedon, P. C., and Begley, T. J.
506 (2010) A Quantitative Systems Approach Reveals Dynamic Control of tRNA Modifications
507 during Cellular Stress. *PLoS Genet.* **6**, e1001247
- 508 31. Su, D., Chan, C. T. Y., Gu, C., Lim, K. S., Chionh, Y. H., McBee, M. E., Russell, B. S., Babu,
509 I. R., Begley, T. J., and Dedon, P. C. (2014) Quantitative analysis of ribonucleoside
510 modifications in tRNA by HPLC-coupled mass spectrometry. *Nat. Protoc.* **9**, 828–841
- 511 32. Kellner, S., Ochel, A., Th, K., Spenkuch, F., Neumann, J., Sharma, S., Entian, K., Schneider,
512 D., and Helm, M. (2014) Absolute and relative quantification of RNA modifications via
513 biosynthetic isotopomers. 10.1093/nar/gku733
- 514 33. Heiss, M., Hagelskamp, F., Marchand, V., Motorin, Y., and Kellner, S. (2021) Cell culture
515 NAIL-MS allows insight into human tRNA and rRNA modification dynamics in vivo. *Nat.*
516 *Commun.* 10.1038/s41467-020-20576-4
- 517 34. Endres, L., Dedon, P. C., and Begley, T. J. (2015) Codon-biased translation can be regulated
518 by wobble-base tRNA modification systems during cellular stress responses. *RNA Biol.* **12**,
519 603–614
- 520 35. Suzuki, T., Suzuki, T., Wada, T., Saigo, K., and Watanabe, K. (2002) Taurine as a constituent

- 521 of mitochondrial tRNAs: new insights into the functions of taurine and human mitochondrial
522 diseases. *EMBO J.* **21**, 6581–9
- 523 36. Zhao, W., He, X., Hoadley, K. A., Parker, J. S., Hayes, D. N., and Perou, C. M. (2014)
524 Comparison of RNA-Seq by poly (A) capture, ribosomal RNA depletion, and DNA microarray
525 for expression profiling. *BMC Genomics.* **15**, 1–11
- 526 37. Cui, P., Lin, Q., Ding, F., Xin, C., Gong, W., Zhang, L., Geng, J., Zhang, B., Yu, X., Yang, J.,
527 Hu, S., and Yu, J. (2010) A comparison between ribo-minus RNA-sequencing and polyA-
528 selected RNA-sequencing. *Genomics.* **96**, 259–265
- 529 38. Wei, C. M., Gershowitz, A., and Moss, B. (1975) Methylated nucleotides block 5' terminus of
530 HeLa cell messenger RNA. *Cell.* **4**, 379–386
- 531 39. Chen-Kiang, S., Nevins, J. R., and Darnell, J. E. (1979) N-6-methyl-adenosine in adenovirus
532 type 2 nuclear RNA is conserved in the formation of messenger RNA. *J. Mol. Biol.* **135**, 733–
533 752
- 534 40. Sommer, S., Lavi, U., and Darnell, J. E. (1978) The absolute frequency of labeled N-6-
535 methyladenosine in HeLa cell messenger RNA decreases with label time. *J. Mol. Biol.* **124**,
536 487–499
- 537 41. Jang, C., Chen, L., and Rabinowitz, J. D. (2018) Metabolomics and Isotope Tracing. *Cell.* **173**,
538 822–837
- 539 42. Kelleher, J. K. (2001) Flux Estimation Using Isotopic Tracers: Common Ground for Metabolic
540 Physiology and Metabolic Engineering. *Metab. Eng.* **3**, 100–110
- 541 43. Buescher, J. M., Antoniewicz, M. R., Boros, L. G., Burgess, S. C., Brunengraber, H., Clish, C.
542 B., DeBerardinis, R. J., Feron, O., Frezza, C., Ghesquiere, B., Gottlieb, E., Hiller, K., Jones, R.
543 G., Kamphorst, J. J., Kibbey, R. G., Kimmelman, A. C., Locasale, J. W., Lunt, S. Y.,
544 Maddocks, O. D. K., Malloy, C., Metallo, C. M., Meuillet, E. J., Munger, J., Nöh, K.,
545 Rabinowitz, J. D., Ralser, M., Sauer, U., Stephanopoulos, G., St-Pierre, J., Tennant, D. A.,
546 Wittmann, C., Vander Heiden, M. G., Vazquez, A., Vousden, K., Young, J. D., Zamboni, N.,
547 and Fendt, S. M. (2015) A roadmap for interpreting ¹³C metabolite labeling patterns from
548 cells. *Curr. Opin. Biotechnol.* **34**, 189–201
- 549 44. Abelson, H. T., Johnson, L. F., Penman, S., and Green, H. (1974) Changes in Rna in Relation
550 to Growth of Fibroblast .2. Lifetime of Messenger-Rna, Ribosomal-Rna, and Transfer-Rna in
551 Resting and Growing Cells. *Cell.* **1**, 161–165
- 552 45. Ross, J. (1995) mRNA Stability in Mammalian Cells. **59**, 423–450
- 553 46. Rana, A. K., and Ankri, S. (2016) Reviving the RNA world: An insight into the appearance of
554 RNA methyltransferases. *Front. Genet.* **7**, 1–9
- 555 47. Boccaletto, P., Machnicka, M. A., Purta, E., Piątkowski, P., Bagiński, B., Wirecki, T. K., de
556 Crécy-Lagard, V., Ross, R., Limbach, P. A., Kotter, A., Helm, M., and Bujnicki, J. M. (2018)
557 MODOMICS: a database of RNA modification pathways. 2017 update. *Nucleic Acids Res.* **46**,
558 D303–D307
- 559 48. Keith, J. M., Ensinger, M. J., and Moss, B. (1978) HeLa cell RNA(2'-O-methyladenosine-N6-
560)-methyltransferase specific for the capped 5'-end of messenger RNA. *J. Biol. Chem.* **253**,
561 5033–5039
- 562 49. Safra, M., Sas-Chen, A., Nir, R., Winkler, R., Nachshon, A., Bar-Yaacov, D., Erlacher, M.,
563 Rossmann, W., Stern-Ginossar, N., and Schwartz, S. (2017) The m1A landscape on cytosolic
564 and mitochondrial mRNA at single-base resolution. *Nature.* **551**, 251–255
- 565 50. Li, X., Xiong, X., Zhang, M., Wang, K., and Chen, Y. (2017) Base-resolution mapping reveals
566 distinct m1A methylome in nuclear- and mitochondrial-encoded transcripts
- 567 51. Kinnaird, A., Zhao, S., Wellen, K. E., and Michelakis, E. D. (2016) Metabolic control of
568 epigenetics in cancer. *Nat. Rev. Cancer.* **16**, 694–707
- 569 52. Gerken, T., Girard, C. A., Tung, Y.-C. L., Webby, C. J., Saudek, V., Hewitson, K. S., Yeo, G.
570 S. H., McDonough, M. A., Cunliffe, S., McNeill, L. A., Galvanovskis, J., Rorsman, P., Robins,
571 P., Prieur, X., Coll, A. P., Ma, M., Jovanovic, Z., Farooqi, I. S., Sedgwick, B., Barroso, I.,
572 Lindahl, T., Ponting, C. P., Ashcroft, F. M., O'Rahilly, S., and Schofield, C. J. (2007) The
573 obesity-associated FTO gene encodes a 2-oxoglutarate-dependent nucleic acid demethylase.
574 *Science.* **318**, 1469–72
- 575 53. Zheng, G., Dahl, J. A., Niu, Y., Fedorcsak, P., Huang, C.-M. M., Li, C. J., Vågbo, C. B., Shi,

- 576 Y., Wang, W.-L. L., Song, S.-H. H., Lu, Z., Bosmans, R. P. G., Dai, Q., Hao, Y.-J. J., Yang,
577 X., Zhao, W.-M. M., Tong, W.-M. M., Wang, X.-J. J., Bogdan, F., Furu, K., Fu, Y., Jia, G.,
578 Zhao, X., Liu, J., Krokhan, H. E., Klungland, A., Yang, Y.-G. G., and He, C. (2013) ALKBH5
579 Is a Mammalian RNA Demethylase that Impacts RNA Metabolism and Mouse Fertility. *Mol.*
580 *Cell.* **49**, 18–29
- 581 54. Slobodin, B., Han, R., Calderone, V., Vrieland, J. A. F. O., Loayza-puch, F., Elkon, R., Agami,
582 R., and Methylation, N. (2017) Transcription Impacts the Efficiency of mRNA Translation via
583 Co-transcriptional N6-adenosine. *Cell.* **169**, 326-337.e12
- 584 55. Bertero, A., Brown, S., Madrigal, P., Osnato, A., Ortmann, D., Yiangou, L., Kadiwala, J.,
585 Hubner, N. C., De Los Mozos, I. R., Sadée, C., Lenaerts, A. S., Nakanoh, S., Grandy, R.,
586 Farnell, E., Ule, J., Stunnenberg, H. G., Mendjan, S., and Vallier, L. (2018) The SMAD2/3
587 interactome reveals that TGF β controls m6A mRNA methylation in pluripotency. *Nature.*
588 **555**, 256–259
- 589 56. Huang, H., Weng, H., Zhou, K., Wu, T., Zhao, B. S., Sun, M., Chen, Z., Deng, X., Xiao, G.,
590 Auer, F., Klemm, L., Wu, H., Zuo, Z., Qin, X., Dong, Y., Zhou, Y., Qin, H., Tao, S., Du, J.,
591 Liu, J., Lu, Z., Yin, H., Mesquita, A., Yuan, C. L., Hu, Y.-C., Sun, W., Su, R., Dong, L., Shen,
592 C., Li, C., Qing, Y., Jiang, X., Wu, X., Sun, M., Guan, J.-L., Qu, L., Wei, M., Müschen, M.,
593 Huang, G., He, C., Yang, J., and Chen, J. (2019) Histone H3 trimethylation at lysine 36 guides
594 m6A RNA modification co-transcriptionally. *Nature.* **567**, 414–419
- 595 57. Koš, M., and Tollervey, D. (2010) Yeast Pre-rRNA Processing and Modification Occur
596 Cotranscriptionally. *Mol. Cell.* **37**, 809–820
- 597 58. Heiss, M., Reichle, V. F., and Kellner, S. (2017) Observing the fate of tRNA and its
598 modifications by nucleic acid isotope labeling mass spectrometry: NAIL-MS. *RNA Biol.* **14**,
599 1260–1268
- 600 59. Wolfe, M. B., Goldstrohm, A. C., and Freddolino, P. L. (2019) Global analysis of RNA
601 metabolism using bio-orthogonal labeling coupled with next-generation RNA sequencing.
602 *Methods.* **155**, 88–103
- 603 60. Macallan, D. C., Fullerton, C. A., Neese, R. A., Haddock, K., Park, S. S., and Hellerstein, M.
604 K. (1998) Measurement of cell proliferation by labeling of DNA with stable isotope-labeled
605 glucose: Studies in vitro, in animals, and in humans. *Proc. Natl. Acad. Sci. U. S. A.* **95**, 708–
606 713
- 607 61. Defoiche, J., Zhang, Y., Lagneaux, L., Pettengell, R., Hegedus, A., Willems, L., and Macallan,
608 D. C. (2009) Measurement of Ribosomal RNA Turnover In Vivo by Use of Deuterium-
609 Labeled Glucose. *Clin. Chem.* **55**, 1824–1833
- 610 62. Busch, R., Neese, R. A., Awada, M., Hayes, G. M., and Hellerstein, M. K. (2007)
611 Measurement of cell proliferation by heavy water labeling. *Nat. Protoc.* **2**, 3045–3057
- 612 63. Maddocks, O. D. K., Labuschagne, C. F., Adams, P. D., and Vousden, K. H. (2016) Serine
613 Metabolism Supports the Methionine Cycle and DNA/RNA Methylation through De Novo
614 ATP Synthesis in Cancer Cells. *Mol. Cell.* **61**, 210–221
- 615 64. Perez, J. F., and Reeds, P. J. (1998) A New Stable Isotope Method Enables the Simultaneous
616 Measurement of Nucleic Acid and Protein Synthesis In Vivo in Mice. *J. Nutr.* **128**, 1562–1569
- 617 65. Fairbanks, L. D., Bofill, M., Ruckemann, K., and Simmonds, H. A. (1995) Importance of
618 ribonucleotide availability to proliferating T-lymphocytes from healthy humans:
619 Disproportionate expansion of pyrimidine pools and contrasting effects of de novo synthesis
620 inhibitors. *J. Biol. Chem.* **270**, 29682–29689
- 621 66. Nikolov, E. N., and Dabeva, M. D. (1985) Re-utilization of pyrimidine nucleotides during rat
622 liver regeneration. *Biochem. J.* **228**, 27–33
- 623 67. Schwanhäusser, B., Busse, D., Li, N., Dittmar, G., Schuchhardt, J., Wolf, J., Chen, W., and
624 Selbach, M. (2011) Global quantification of mammalian gene expression control. *Nature.* **473**,
625 337–42
- 626 68. Tani, H., Mizutani, R., Salam, K. A., Tano, K., Ijiri, K., Wakamatsu, A., Isogai, T., Suzuki, Y.,
627 and Akimitsu, N. (2012) Genome-wide determination of RNA stability reveals hundreds of
628 short-lived noncoding transcripts in mammals. *Genome Res.* **22**, 1382
- 629 69. Ramanathan, A., Robb, G. B., and Chan, S. H. (2016) mRNA capping: Biological functions
630 and applications. *Nucleic Acids Res.* **44**, 7511–7526

- 631 70. Galloway, A., and Cowling, V. H. (2019) mRNA cap regulation in mammalian cell function
632 and fate. *Biochim. Biophys. Acta - Gene Regul. Mech.* **1862**, 270–279
- 633 71. Zhang, L. S., Liu, C., Ma, H., Dai, Q., Sun, H. L., Luo, G., Zhang, Z., Zhang, L., Hu, L., Dong,
634 X., and He, C. (2019) Transcriptome-wide Mapping of Internal N7-Methylguanosine
635 Methylome in Mammalian mRNA. *Mol. Cell.* **74**, 1304-1316.e8
- 636 72. Squires, J. E., Patel, H. R., Nusch, M., Sibbritt, T., Humphreys, D. T., Parker, B. J., Suter, C.
637 M., and Preiss, T. (2012) Widespread occurrence of 5-methylcytosine in human coding and
638 non-coding RNA. *Nucleic Acids Res.* **40**, 5023–5033
- 639 73. Lafontaine, D., Delcour, J., Glasser, A. L., Desgrès, J., and Vandenhoute, J. (1994) The DIM1
640 gene responsible for the conserved m26Am26A dimethylation in the 3'-terminal loop of 18 S
641 rRNA is essential in yeast. *J. Mol. Biol.* **241**, 492–497
- 642 74. O'Sullivan, M., Rutland, P., Lucas, D., Ashton, E., Hendricks, S., Rahman, S., and Bitner-
643 Glindzicz, M. (2015) Mitochondrial m.1584A 12S m62A rRNA methylation in families with
644 m.1555A>G associated hearing loss. *Hum. Mol. Genet.* **24**, 1036–44
- 645 75. Chan, C. T. Y., Chionh, Y. H., Ho, C. H., Lim, K. S., Babu, I. R., Ang, E., Wenwei, L.,
646 Alonso, S., and Dedon, P. C. (2011) Identification of N6,N6-dimethyladenosine in transfer
647 RNA from *Mycobacterium bovis* bacille calmette-guerin. *Molecules.* **16**, 5168–5181
- 648 76. McCloskey, J. a, Graham, D. E., Zhou, S., Crain, P. F., Ibba, M., Konisky, J., Söll, D., and
649 Olsen, G. J. (2001) Post-transcriptional modification in archaeal tRNAs: identities and
650 phylogenetic relations of nucleotides from mesophilic and hyperthermophilic
651 Methanococcales. *Nucleic Acids Res.* **29**, 4699–4706
- 652 77. Ensfelder, T. T., Kurz, M. Q., Iwan, K., Geiger, S., Matheisl, S., Müller, M., Beckmann, R.,
653 and Carell, T. (2018) ALKBH5-induced demethylation of mono- and dimethylated adenosine.
654 *Chem. Commun. (Camb).* **54**, 8591–8593
- 655 78. Goberdhan, D. C. I., Wilson, C., and Harris, A. L. (2016) Amino Acid Sensing by mTORC1:
656 Intracellular Transporters Mark the Spot. *Cell Metab.* **23**, 580–589
- 657 79. Fu, Y., Jia, G., Pang, X., Wang, R. N., Wang, X., Li, C. J., Smemo, S., Dai, Q., Bailey, K. A.,
658 Nobrega, M. A., Han, K.-L., Cui, Q., and He, C. (2013) FTO-mediated formation of N6-
659 hydroxymethyladenosine and N6-formyladenosine in mammalian RNA. *Nat. Commun.* **4**,
660 1798
- 661 80. Mauer, J., and Jaffrey, S. R. (2018) FTO, m⁶A, and the hypothesis of reversible
662 epitranscriptomic mRNA modifications. *FEBS Lett.* **592**, 2012–2022
- 663 81. MacLean, B., Tomazela, D. M., Shulman, N., Chambers, M., Finney, G. L., Frewen, B., Kern,
664 R., Tabb, D. L., Liebler, D. C., and MacCoss, M. J. (2010) Skyline: an open source document
665 editor for creating and analyzing targeted proteomics experiments. *Bioinformatics.* **26**, 966–
666 968
- 667 82. Fets, L., Driscoll, P. C., Grimm, F., Jain, A., Nunes, P. M., Gounis, M., Doglioni, G.,
668 Papageorgiou, G., Ragan, T. J., Campos, S., Silva Dos Santos, M., MacRae, J. I., O'Reilly, N.,
669 Wright, A. J., Benes, C. H., Courtney, K. D., House, D., and Anastasiou, D. (2018) MCT2
670 mediates concentration-dependent inhibition of glutamine metabolism by MOG. *Nat. Chem.*
671 *Biol.* **14**, 1032–1042
672

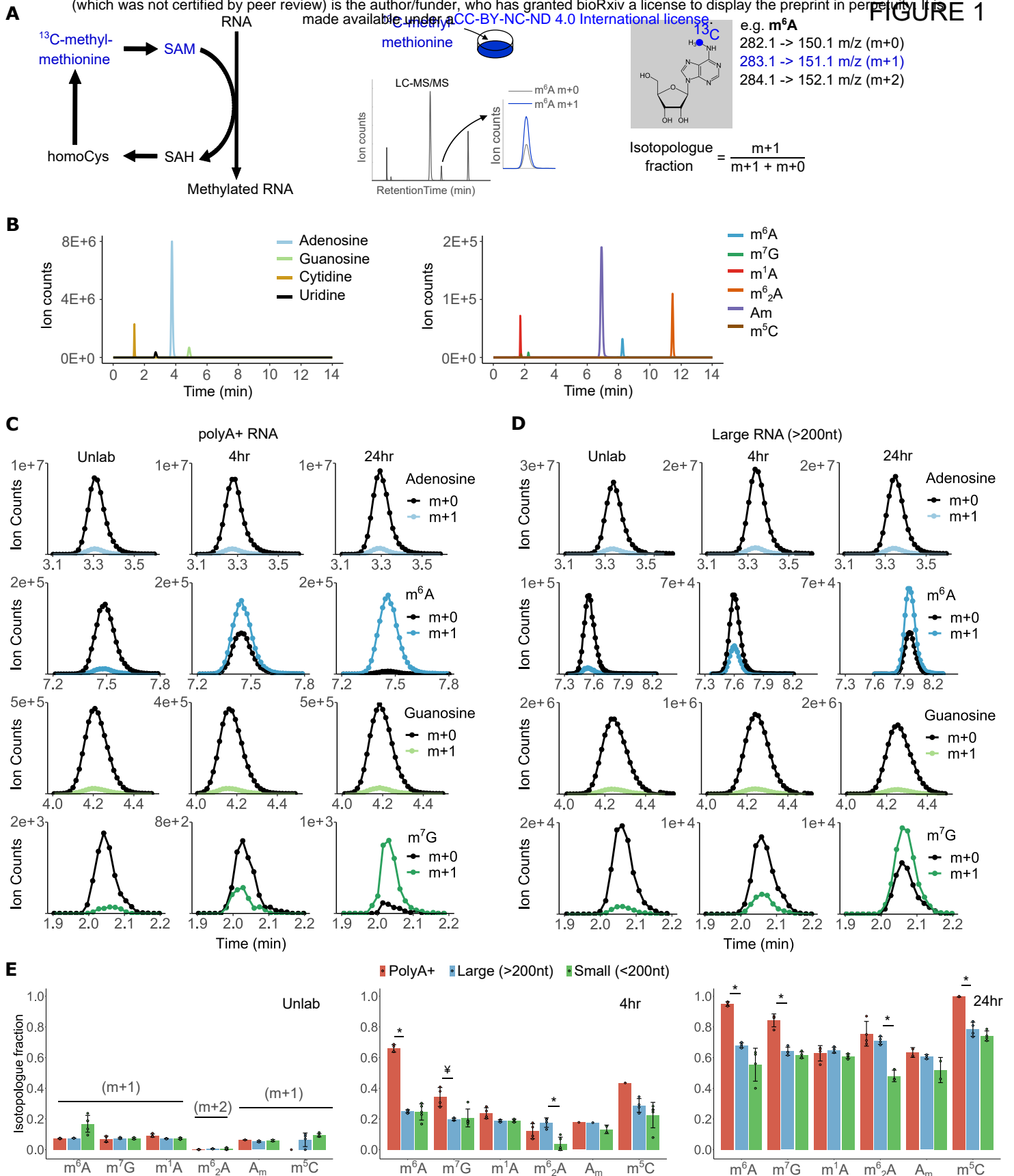


Figure 1. ^{13}C labelling of RNA modifications across RNA classes. (A) The ^{13}C -dynamods workflow shows the tracing of RNA methylation: cells are cultured with [^{13}C -methyl]-methionine, the RNA is isolated, digested to ribonucleosides and subjected to LC-MS/MS analysis. The isotopologues detected for m^6A are shown. (B) Representative chromatogram of unmodified and modified ribonucleosides from total RNA. (C-D) The $\text{m}+0$ and $\text{m}+1$ isotopologues of modified and unmodified ribonucleosides (representative chromatograms) in polyA+ (C) and large RNA (D). (E) Quantification of the isotopologue fractions of each ribonucleoside in polyA+, large and tRNA under unlabelled ('Unlab') conditions, after 4 and 24 hours of culture with [^{13}C -methyl]-methionine. m^6A , N^6 -methyladenosine; m^7G , 7-methylguanosine; m^1A , 1-methyladenosine; m^6_2A , N^6,N^6 -dimethyladenosine; Am , 2'-O-methyladenosine; m^5C , 5-methylcytosine; m^1G , 1-methylguanosine; m^2G , 2-methylguanosine. SAM, s-adenosylmethionine; SAH, s-adenosylhomocysteine; homoCys, homocysteine. Error bars represent standard deviation of three to four biological replicates, with the exception of m^5C in polyA+-purified RNA (two replicates at 24hr, one replicate in the Unlab/4hr time points). In all cases, each replicate is the average of two technical replicas. * denotes $P < 0.005$, † denotes $P < 0.05$, of a two-sided Student's t-Test comparing samples as indicated.

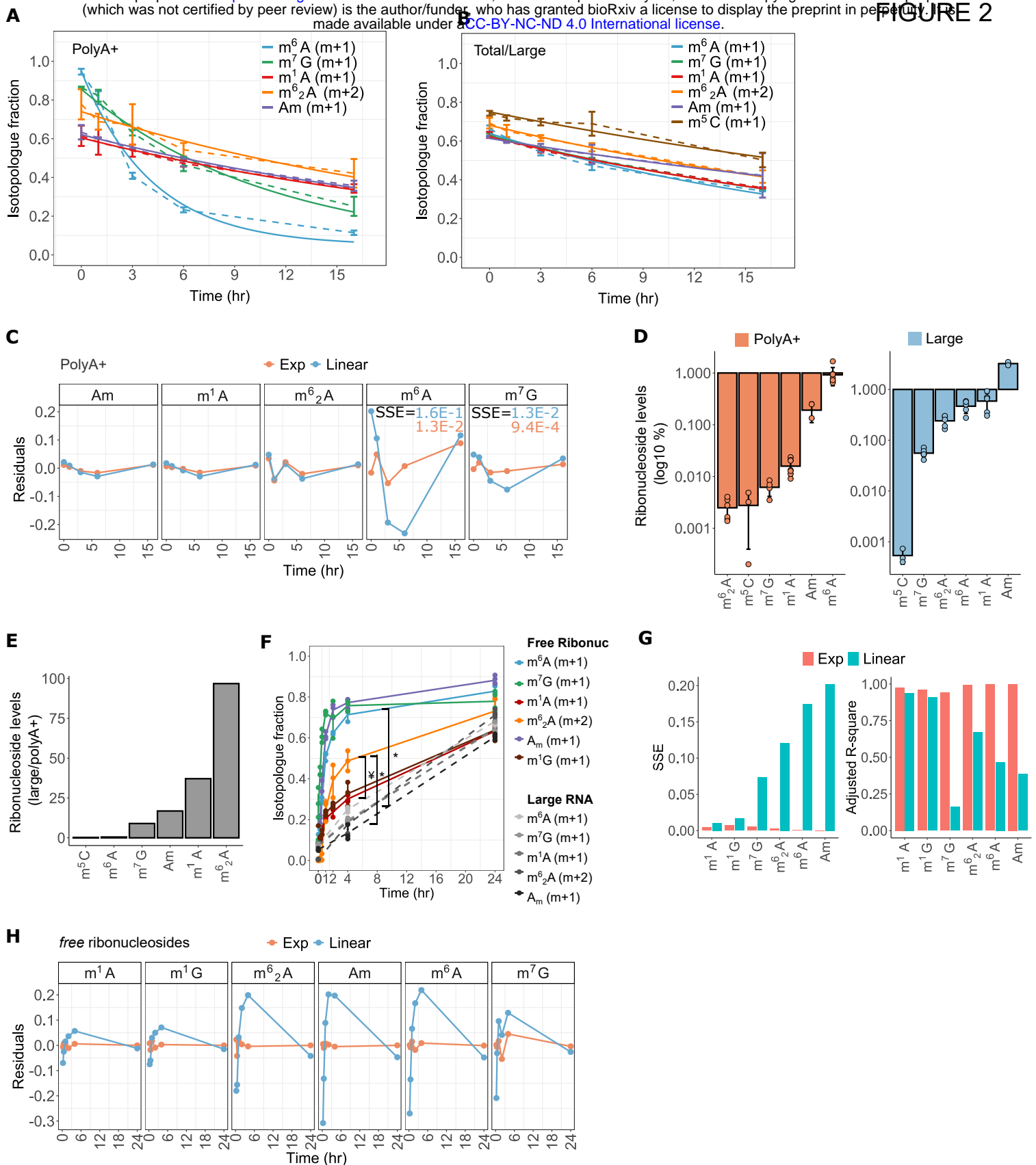


Figure 2. Turnover of modified ribonucleosides in polyA+, ncRNA and free ribonucleoside pool. (A-B) Isotopologue fractions during the ‘chase’ of ¹³C-labelled modifications with naturally labelled methionine for 0, 1, 3, 6 and 16 hours, in polyA+ (A) and total/large RNA (B); dashed lines connect data points; solid lines, exponential (A) or linear (B) fit of isotopologue fractions. (C) Residuals of a linear vs. exponential regression of isotopologue fractions in polyA+ RNA in the chase experiment. (D) Normalized ion counts of modified ribonucleosides relative to the ion counts sum of all ribonucleosides, shown for polyA+ and large RNA. (E) Ratio of normalised ion counts between polyA+ and large RNA, as determined in (D). (F) Isotopologue fraction of free ribonucleosides analysed from metabolic extracts; grey datapoints refer to large RNA modifications (Fig. 1E) for comparison. (G-H) Goodness-of-fit of a linear vs. exponential fit of the isotopologue fractions in free modified ribonucleosides. SSE, sum of squared errors. m^6A , N6-methyladenosine; m^7G , 7-methylguanosine; m^1A , 1-methyladenosine; m^6_2A , N6,N6-dimethyladenosine; A_m , 2'-O-methyladenosine; m^5C , 5-methylcytidine; m^1G , 1-methylguanosine; A, adenosine; G, guanosine. Error bars represent 90% confidence intervals in (a-b), or standard deviation in (d, f) of at least three biological replicates with exception of A_m (two replicates). In all cases, each replicate is the average of two technical replicas. * denotes $P < 0.005$, † denotes $P < 0.05$, of a two-sided Student’s t-Test comparing m^6_2A and m^6A in the free ribonucleoside pool (free ribonuc) to large RNA, or m^6_2A to m^1A in the free ribonuc pool.

